Electrochemical sulfidation of WS$_2$ nanoarrays

Escalera-López, Daniel; Griffin, Ross; Isaacs, Mark; Wilson, Karen; Palmer, Richard E.; Rees, Neil V.

Link to publication on Research at Birmingham portal

CrossMark

Electrochemical sulfidation of WS$_2$ nanoarrays: Strong dependence of hydrogen evolution activity on transition metal sulfide surface composition

Daniel Escalera-López[a,b], Ross Griffin[b], Mark Isaacs[c], Karen Wilson[c], Richard E. Palmer[d], Neil V. Rees[a,*]

[a] Centre for Hydrogen and Fuel Cell Research, School of Chemical Engineering, University of Birmingham, Birmingham B15 2TT, UK
[b] School of Physics and Astronomy, University of Birmingham, Birmingham B15 2TT, UK
[c] European Bioenergy Research Institute, Aston University, Birmingham B4 7ET, UK
[d] College of Engineering, Swansea University, Fabian Way, Swansea SA1 8EN, UK

A B S T R A C T

The activity of transition metal sulfides for the hydrogen evolution reaction (HER) can be increased by sulfur-enrichment of active metal-sulfide sites. In this report, we investigate the electrochemical sulfidation of atmospherically aged WS$_2$ nanoarrays with respect to enhancing HER activity. In contrast to MoS$_2$, it is found that sulfidation diminishes HER activity. Electrochemical and XPS experiments suggest the involvement of insoluble tungsten oxides in the altered HER and electron transfer properties. This demonstrates the strong dependence of the transition metal dichalcogenide (TMD) composition with the successful sulfur incorporation and subsequent HER activity.

1. Introduction

The demand for sustainable sources of electrochemical hydrogen production [1] has triggered the development of the abundant and low-cost TMDs as substitutes to the best performing platinum group metal catalysts for the hydrogen evolution reaction (HER) [2–5].

To improve their HER activity, research has focussed on the preparation of S-rich TMD structures which surpass the 1:2 M:X stoichiometry found in bulk materials [6–8]. Such sulfur enrichment aims to incorporate more bridging S_2^{2-} and terminal S^{2-} moieties into the TMD structure; both consistently reported as being the active sites involved in proton adsorption and desorption [9,10]. Enhanced HER performance has been reported for S-rich structures such as amorphous MoS$_{2+x}$ [11–15] and WS$_{2.64}$ electrodeposited thin films [9], as well as on wet chemical synthesis-prepared MoS$_{2+x}$ [16,17] or MX$_3$/MX$_2$ physical mixtures [18]. However, some of the proposed structures exhibit diminished HER performances after atmospheric or electrochemically-induced sulfur depletion [14,18] or impurities presence [19].

We report the use of a one step, room temperature electrochemical sulfidation method initially developed for MoS$_2$ [20], for sulfur-enriching WS$_2$. In particular, atmospherically-aged WS$_2$ nanocone arrays which are of interest due to their enhanced electrocatalytic properties [21]. Changes in the electrocatalytic behaviour are understood via monitoring surface composition, morphology, and electron transfer properties over a one month period by XPS, SEM, and voltammetric experiments.

2. Materials and methods

2.1. Fabrication

The plasma-etch fabrication method used is based on a literature method [22–24], recently reported in TMDs for electrocatalytic applications [20,21,25].

In short, WS$_2$ (defect-free, 99.9995% purity, 2D Semiconductors USA) crystals cut into rectangles of approximately 1.5 × 5 mm were affixed to glassy carbon (GC) type 2 stubs (7 mm diameter, 2 mm thick, Alfa Aesar, UK) with carbon tape. A 20 μL mixture of a 216 ± 4 nm diameter polystyrene-latex nanosphere (NS) suspension (3000 Series Nanosphere, 1 wt% in water, Thermo Scientific, UK) with absolute ethanol in a 1:1 vol. ratio was transferred to a silicon wafer (previously cleaned with piranha solution and oxygen plasma) to form a self-assembled, hexagonal close-packed, NS monolayer. The NS monolayer was transferred onto the liquid interface of a water-filled Petri dish containing the TMD-modified GC stubs, and the supernatant extracted with a syringe to promote NS deposition onto the TMD surface.

NS-modified TMDs etching was carried out in an Oxford

Instruments Plasmalab NGP 80 ICP/RF etcher. Isotropic oxygen plasma etching (40 s, 30 sccm O_2 flow rate, 100 W RF power) was performed as an NS shrinking step. Afterwards, exposure to an anisotropic plasma etching mixture of SF_6/C_4F_8 (20 sccm/30 sccm, 200 W ICP, 20 W RF power) for variable times (15–60 s) was carried out to obtain nanocone arrays with variable aspect ratios. Pressures of 15 mTorr and temperatures of 20 °C were used in both etching steps. SEM micrographs of the electrochemically tested samples before/after sulfidation were acquired to determine the aspect ratio (nanocone height/base diameter), interspacing, and dimensionless radial (R, domain radius/nanocone radius) and normal (Z, nanocone height/nanocone radius) coordinates [26] of the individual nanostructures in the array (XL 30 SFEG and JEOL 7100 FEG-SEM, 5 kV, tilt angles from 45° to 85°).

2.2. Electrochemical characterization

Electrochemical measurements were carried out with a PC-controlled PGSTAT128N potentiostat (Metrohm Autolab B·V, Netherlands) in a thermostatted three-electrode electrochemical cell (23 ± 2 °C). The electrodes used were: a bright Pt mesh counter (Alfa Aesar Ltd., UK), a double junction saturated Ag/AgCl reference (electrochemical sulfidation experiments, Sigma-Aldrich), a saturated calomel (SCE) reference electrode (HER experiments, BAS Inc., Japan) and TMD-modified GC stubs connected to a rotating disk working electrode (OrigaLys ElectroChem SAS, France).

HER experiments were carried out in a 2 mM $HClO_4$ (ACS ≥ 70%, Sigma-Aldrich), 0.1 M $NaClO_4$ (ACS ≥ 98%, Sigma-Aldrich) solution using a range of voltage scan rates (2–1200 mV s^{-1}). Preconditioning of TMD electrodes prior to HER experiments was via 10 cycles from − 0.045 to − 1.645 V (vs SCE) at a voltage scan rate of 50 mV s^{-1}. Additional capacitance (voltage range − 0.2 to 0.2 V vs. NHE, scan rates 10–500 mV s^{-1}) and impedance measurements (voltage range 0 to − 1.645 V vs. SCE, frequency range 10^{-1} to 10^5 Hz, voltage amplitude 10 mV) were performed alongside all HER measurements to apply roughness factor and iR compensation corrections. HER potentials are referenced versus the normal hydrogen electrode (NHE) by means of Nernstian shift correction ($E_{NHE} = 0.242$ V + 0.059 pH).

Investigation of heterogeneous electron transfer (HET) rates was performed under the same conditions as of Pumera et al. for ease of reference [5,13], by acquiring five CVs in 10 mM K4Fe(CN)6/K3Fe(CN)6 (BioUltra ≥ 99.5%, Sigma-Aldrich) electrolyte supported by a pH 7.2 phosphate buffer (50 mM potassium phosphate monobasic/potassium phosphate dibasic trihydrate, ≥ 99%, Sigma-Aldrich) at scan rates from 10 to 300 mV s^{-1}. Experimental HET rate constants (k_{app}^O) were calculated by correlating the peak-to-peak separation of the Fe(CN)$_6^{4-}$/Fe(CN)$_6^{3-}$ redox couple with the dimensionless parameter ψ, using the literature methods of Nicholson and Shain ($\psi \approx 0.1$ and $\Delta E_P < 210$ mV) [27], and Klinger and Kochi ($\psi < 0.1$ and $\Delta E_P > 210$ mV) [28]. A diffusion coefficient of 7.26×10^{-6} cm^2 s^{-1} for the [Fe(CN)6]$^{4-/3-}$ redox pair was used in the calculation [29], assuming $\alpha = 0.5$ For the nanoarrays under study, Case 4 diffusion behaviour (1D) was observed [30]. All electrolytes were freshly prepared with ultrapure water (resistivity not < 18.2 MΩ·cm, Millipore Milli-Q Direct 8), and thoroughly purged with N_2 (Oxygen-free grade, BOC Gases plc), and experiments run under a N_2 atmosphere. All glassware was cleaned with a dilute solution of $KMnO_4$ in concentrated H_2SO_4 followed by rinsing with ultrapure water.

2.3. XPS measurements

A Kratos Axis HSi X-ray photoelectron spectrophotometer (Aston University) fitted with a charge neutraliser and operated using a Mg Kα (1253.6 eV) achromatic radiation, was used to record spectra at a pressure of < 1×10^{-9} Torr using a spot size of 100 μm. Pass energies used were: 160 eV for survey spectra, and 20 eV for high resolution scans of specific energy regions. Data processing was performed using CASA XPS version 2.3.18PR1.0, with spectral energy corrected to the adventitious C 1 s peak at 284.6 eV. Shirley backgrounds were applied to high resolution peaks before being fitted with individual components. W 4f spectra were fit using a FWHM of 0.98 eV, peak area ratios of 4:3, doublet separations of 2.17 eV and Gaussian-Lorentz (30) lineshape, with W 4f$_{7/2}$ WS2 2H (32.7 eV), W 4f$_{7/2}$ WS$_2$ 1 T (31.7 eV) and W 4f$_{7/2}$ WO$_2$ (33.1 eV) components, whilst the overlapping W 5p$_{3/2}$ feature was fitted with a FWHM of 2 eV, a Gaussian-Lorentz (30) lineshape and a binding energy of 38.1 eV. Sulfur 2p peaks were fitted with a FWHM of 1.03 eV, peak area ratios of 2:1 and a binding energy for S 2p$_{3/2}$ WS$_2$ of 162.3 eV [31,32].

3. Results and discussion

For reinstating, or improving, the initial HER activity of atmospherically-exposed WS$_2$ samples, a solution-phase method previously demonstrated for MoS$_2$ nanoarrays [20] was used. This requires voltage cycling of the TMD samples in a pH 3 solution containing 10 mM $Na_2S_2O_3$ and 0.1 M Na_2SO_4 whereby $S_2O_3^{2-}$ spontaneously decomposes to form colloidal sulfur [33].

$$S_2O_3^{2-} (aq) + H^+ (aq) \rightleftharpoons S (s) + HSO_3^-$$
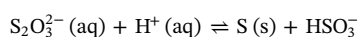
An anodic sweep to fully oxidize the TMD surface, was followed by a cathodic scan to maximize sulfur incorporation onto the TMD surface by reduction

$$S (s) + 2e^- \rightleftharpoons + S^{2-} (aq)$$
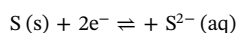
For MoS$_2$, electrochemically-induced surface oxidation (at E > + 1 V vs Ag/AgCl) yields the acid-soluble MoO$_4^{2-}$ species [34]. Sulfur incorporation after surface oxidation suggests that MoO$_4^{2-}$ species assist in the overall sulfidation mechanism. For WS$_2$, the cyclic voltammogram obtained during the sulfidation treatment is similar to that of MoS$_2$ [20].

The application of this method to WS$_2$ was evaluated by monitoring HER performance, oxidation state, and electron transfer properties over a one month period following this sulfidation treatment on previously tested, atmospherically aged WS$_2$ samples. This provided the following observations: (i) freshly sulfidated samples did not necessarily present enhanced HER performances compared with pre-sulfidated samples, and (ii) the samples' HER peak current, after correction for roughness factor, was inferior after a 3-week environmental exposure compared to the pre-sulfidated, atmospherically-exposed state.

Both phenomena can be understood by changes in oxidation state revealed by XPS. For the 31 ± 1 s ($R = 2$, $Z = 6.4$) plasma-etched WS$_2$ sample, the peak current decays to half of its initial value following sulfidation (Fig. 1a). This is correlated to a decrease in the total S:W ratio (from ca. 2:1 to 1.5:1, see Fig. 2e), and the appearance of WO$_2$ at the crystal surface up to ca. 24% (W 4f$_{7/2}$/W 4f$_{5/2}$ doublet lies at binding energies of ca. 33 and 35.2 eV, respectively; Figs. 1c, 2a) [31]. Previous reports on bulk and chemically-exfoliated WS$_2$ crystals suggest that incorporation of WO$_2$ is detrimental for the HER [18,35]. In the case of the 31 ± 1 s sample, this is supported by the changed HER kinetics (Tafel slope increase from 100 to 185 mV dec^{-1}, Fig. 3c) and higher onset potentials ($|\eta_{onset}|$ from 173 to 207 mV).

Conversely, the 61 ± 1 s plasma-etched WS$_2$ sample presented higher peak currents (Fig. 1b) and kinetics (Tafel slope 130 vs. initial 210 mV dec^{-1}, Fig. 3d) following sulfidation, despite the decay in the total S:W ratio (from ca. 2:1 to 1.88:1, see Fig. 2f) and the 14% increase in surface WO$_2$ content (Figs. 1d, 2c). This initially non-linear trend is found to be linked to the S:W ratio, if calculated solely using the W^{4+} XPS components characteristic of WS$_2$. Sulfur-rich S:W ratios promote enhanced HER performance and vice versa. Maximum peak currents coincide with the highest sulfur-to-metal ratios for both 31 ± 1 s (S:W = 2.08:1, $j_p \approx 9$ mA cm^{-2}, day 8) and 61 ± 1 s (S:W = 2.18:1, $j \approx 1.6$ mA cm^{-2}, freshly sulfidated) samples. After these peak values, both post-sulfidated 31 ± 1 s and 61 ± 1 s etched samples exhibited
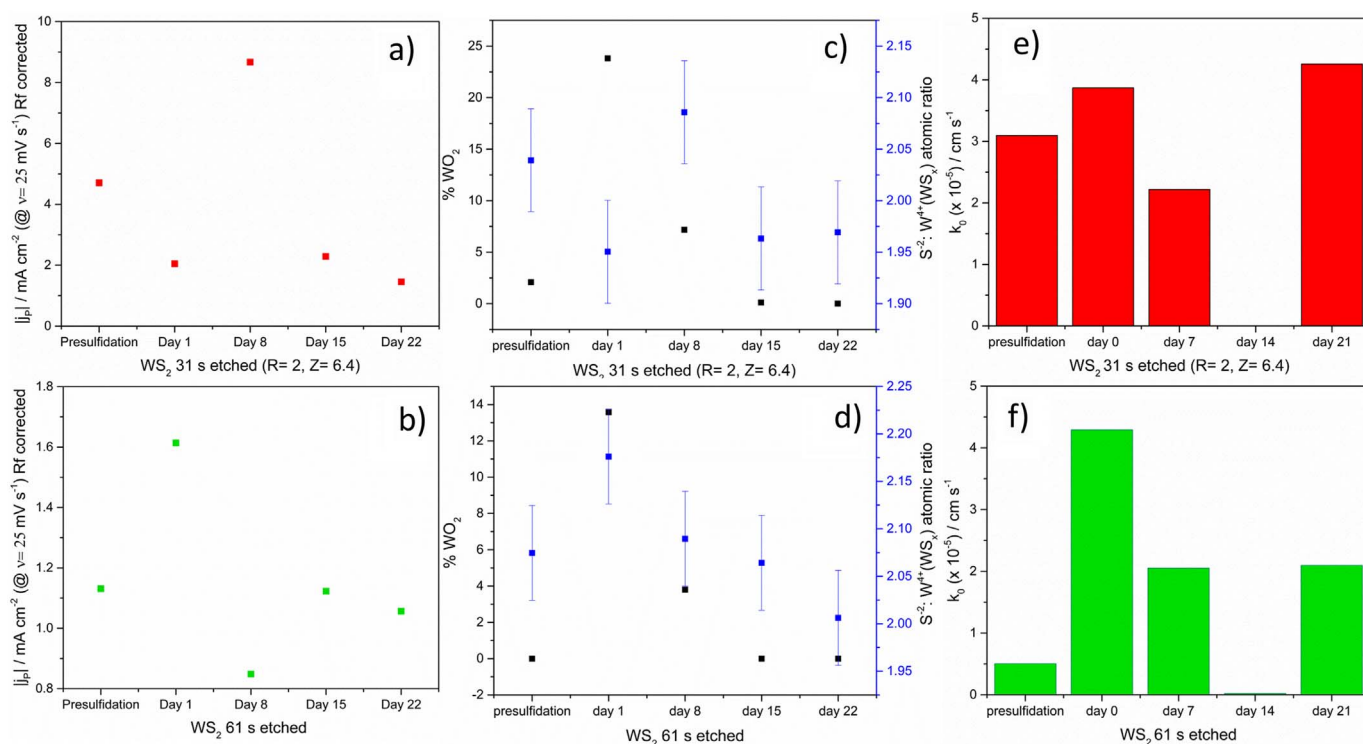
Fig. 1. Comparison of: a)–b) roughness-factor corrected HER peak current densities at υ = 25 mV s^{-1}, c)–d) WO$_2$ surface content (left axis) and S^{2-}:W^{4+} XPS atomic photoemission ratios (right axis), and e)–f) k_{app}^O values for the [Fe(CN)$_6$]$^{4-}$/[Fe(CN)$_6$]$^{3-}$ redox probe, for atmospherically aged, sulfidation treated plasma-etched WS$_2$ samples 31 $\pm$ 1 s (R = 2, Z = 6.4, first row) and 61 $\pm$ 1 s (second row), after weekly electrochemical testing over a three-week ambient exposure period.

an HER current decrease in subsequent electrochemical testing to values lower or comparable with the freshly sulfidated state, due to lower S:W ratios. This accords with previous investigations which correlated higher sulfur content in TMDs with improved hydrogen turnover frequencies [12,14], and sulfur-depleted W-edge sites of electro-oxidised WS$_2$ with poor catalytic activity [35]. We hypothesize that the electrochemically-induced restructuring gradually depletes the WO$_2$ phase, initially exposing underlying WS$_2$ with high active site densities which are later reconstructed during atmospheric and experimental conditions to a more homogeneous nanostructure (Fig. 2g–h).

The cathodic feature appearing at E ca. − 0.4 V vs NHE in the HER experiments (Fig. 3a and b) is ascribed to the diffusion decay peak profile of proton reduction catalysed by the WS$_2$ active sites, characteristic of the fully-supported, low proton concentration electrolyte used [36,37]. Indeed, the resolution of this peak also seems correlated with the S^{2-}:W^{4+} ratio, and consequently to the active sites present.

With regard to the electron transfer kinetics, both samples exhibit higher k_{app}^O values ($\approx$ 4 × 10^{-5} cms^{-1}) after undergoing the sulfidation treatment (Fig. 1e–f). This agrees with literature reports which found enhanced electrical conductivities of WO$_x$ species vs. WS$_2$ [38], beneficial for mediating in the redox chemistry of surface sensitive species such as Fe(CN)$_6^{4-}$/Fe(CN)$_6^{3-}$. A gradual decrease in k_{app}^O values after two weeks of testing correlates with reduced WO$_2$ content at the crystal surface, whereas restored k_{app}^O values after three weeks can be attributed to the higher WS$_2$ metallic 1T polymorph contents (ca. 10–15%).

These results suggest that this sulfidation method does not incorporate sulfur into the atmospherically aged WS$_2$ samples. Instead, it promotes the appearance of WO$_x$ moieties at the WS$_x$ surface which are reduced in the cathodic sweep. We hypothesize that in general, the sulfur incorporation is only effective when the electro-oxidative step of TMDs forms acid-soluble species, as sulfur incorporation into atmospherically-aged MoS$_2$ crystals was optimal when the cathodic voltage vertex surpassed the reduction potential of the TMD oxidised species (MoO$_4^{2-}$) [20]. In the case of WS$_2$, the oxidised WO$_x$ species generated

during the electro-oxidative step are insoluble at pH ≤ 3 [39], coinciding with the optimized pH value for the sulfidation electrolyte (pH 3). Consequently, the electroreduced sulfur cannot be incorporated into the WO$_x$ structure, and would dissolve under acidic conditions [40]. Hence, we predict that the electrochemical solvent-phase sulfidation method is only suited for MoX$_2$ (X = S, Se) rather than for WX$_2$ (X = S, Se).

4. Conclusions

In contrast to MoS$_2$, the application of the solution-phase, room-temperature electrochemical sulfidation method to obtain S-rich structures did not lead to S-rich WS$_x$ but to S-deficient WS$_x$ structures with high WO$_2$ surface content. The inferior HER performances but improved electron transfer properties are in agreement with the detrimental effect reported after WO$_2$ incorporation into WS$_2$ for the HER catalysis. The unsuccessful incorporation of electroreduced sulfide in the WS$_x$ structure is suspected to arise from the nature of the sulfidation mechanism: redeposition of acid-soluble MoO$_4^{2-}$ species for MoX$_2$ improves S^{2-} incorporation onto the surface, which is not possible in the case of WX$_2$ as the WO$_x$ compounds formed are acid insoluble. This demonstrates the key role of the nature of the TMDs in the successful electrochemical incorporation of sulfur in their structure, and reveals that an electrochemistry-based sulfidation method universally applicable for any TMDs remains to be developed.
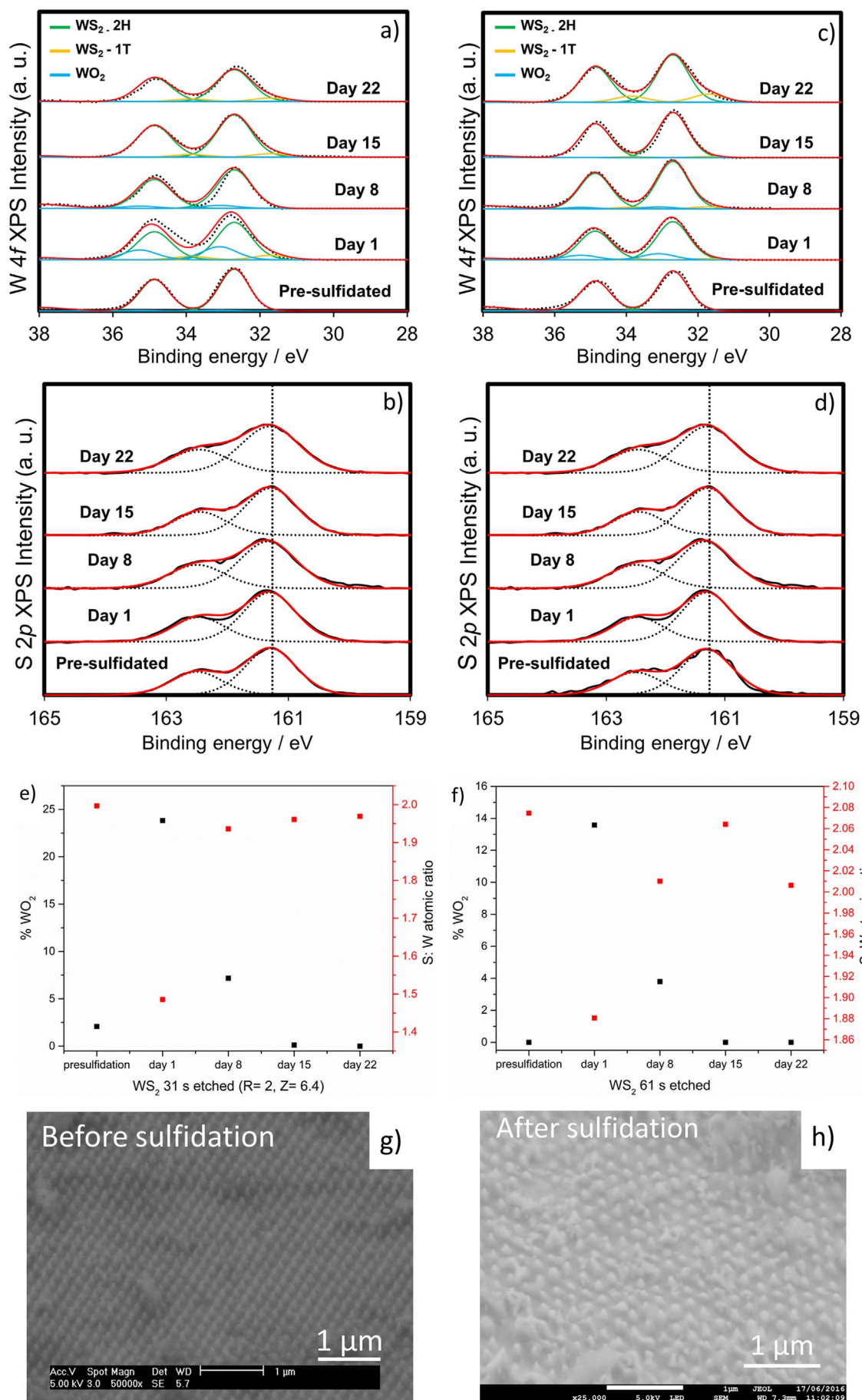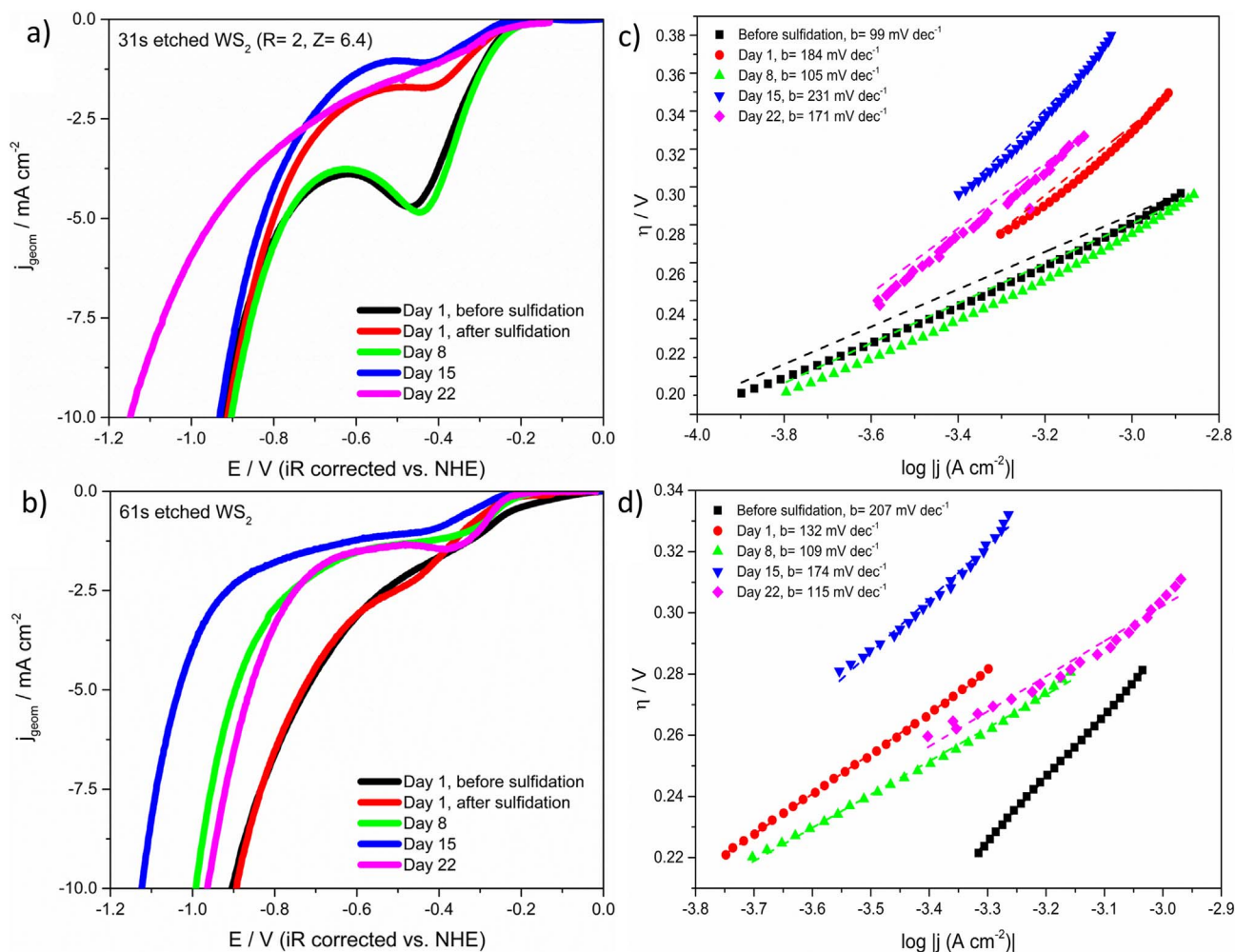
(caption on next page)

Fig. 3. Left column: Linear sweep voltammograms in the 0 to − 1.2 V voltage range of a) 31 ± 1 s (R = 2, Z = 6.4) and b) 61 ± 1 s atmospherically aged, sulfidation treated plasma-etched WS_2 samples over a three week ambient exposure period. Right column: Tafel plots (η vs. $\log|j_{geom}|$) of c) 31 ± 1 s (R = 2, Z = 6.4) and d) 61 ± 1 s atmospherically aged, sulfidation treated plasma-etched WS_2 samples over a three week ambient exposure period. Labels: pre-sulfidated (black), post-sulfidated (red), 8-day atmosphere exposed (green), 15-day atmosphere exposed (blue) and 22-day atmosphere exposed (magenta). (For interpretation of the references to colour in this figure legend, the reader is referred to the web version of this article.)

References

[1] J.A. Turner, Sustainable hydrogen production, Science 305 (2004) 972–974, http://dx.doi.org/10.1126/science.1103197.

[2] P.C.K. Vesborg, B. Seger, I. Chorkendorff, Recent development in hydrogen evolution reaction catalysts and their practical implementation, J. Phys. Chem. Lett. 6 (2015) 951–957, http://dx.doi.org/10.1021/acs.jpclett.5b00306.

[3] W. Choi, N. Choudhary, G.H. Han, J. Park, D. Akinwande, Y.H. Lee, Recent development of two-dimensional transition metal dichalcogenides and their applications, Mater. Today 20 (2017) 116–130, http://dx.doi.org/10.1016/j.mattod.2016.10.002.

[4] I. Roger, M.A. Shipman, M.D. Symes, Earth-abundant catalysts for electrochemical and photoelectrochemical water splitting, Nat. Rev. Chem. 1 (2017) 0003, http://dx.doi.org/10.1038/s41570-016-0003.

[5] Z. He, W. Que, Molybdenum disulfide nanomaterials: structures, properties, synthesis and recent progress on hydrogen evolution reaction, Appl. Mater. Today 3 (2016) 23–56, http://dx.doi.org/10.1016/j.apmt.2016.02.001.

[6] X. Chia, A.Y.S. Eng, A. Ambrosi, S.M. Tan, M. Pumera, Electrochemistry of nanostructured layered transition-metal dichalcogenides, Chem. Rev. 115 (2015) 11941–11966, http://dx.doi.org/10.1021/acs.chemrev.5b00287.

[7] F. Reale, K. Sharda, C. Mattevi, From bulk crystals to atomically thin layers of group VI-transition metal dichalcogenides vapour phase synthesis, Appl. Mater. Today 3 (2016) 11–22, http://dx.doi.org/10.1016/j.apmt.2015.12.003.

[8] S. Li, S. Wang, D.M. Tang, W. Zhao, H. Xu, L. Chu, et al., Halide-assisted atmospheric pressure growth of large WSe_2 and WS_2 monolayer crystals, Appl. Mater. Today 1 (2015) 60–66, http://dx.doi.org/10.1016/j.apmt.2015.09.001.

[9] S.M. Tan, M. Pumera, Bottom-up electrosynthesis of highly active tungsten sulfide ($WS_{3−x}$) films for hydrogen evolution, ACS Appl. Mater. Interfaces 8 (2016) 3948–3957, http://dx.doi.org/10.1021/acsami.5b11109.

[10] B. Hinnemann, P. Moses, J. Bonde, K.P. Jørgensen, J.H. Nielsen, S. Horch, et al., Biomimetic hydrogen evolution: MoS_2 nanoparticles as catalyst for hydrogen evolution, J. Am. Chem. Soc. 127 (2005) 5308–5309 http://pubs.acs.org/doi/abs/10.1021/ja0504690 (accessed August 6, 2015).

[11] D. Merki, S. Fierro, H. Vrubel, X. Hu, Amorphous molybdenum sulfide films as catalysts for electrochemical hydrogen production in water, Chem. Sci. 2 (2011) 1262–1267, http://dx.doi.org/10.1039/C1SC00117E.

[12] H. Vrubel, X. Hu, Growth and activation of an amorphous molybdenum sulfide hydrogen evolving catalyst, ACS Catal. 3 (2013) 2002–2011, http://dx.doi.org/10.1021/cs400441u.

[13] P.D. Tran, T.V. Tran, M. Orio, S. Torelli, Q.D. Truong, K. Nayuki, et al., Coordination polymer structure and revisited hydrogen evolution catalytic mechanism for amorphous molybdenum sulfide, Nat. Mater. 15 (2016) 640–646, http://dx.doi.org/10.1038/nmat4588.

[14] L.R.L. Ting, Y. Deng, L. Ma, Y.J. Zhang, A.A. Peterson, B.S. Yeo, Catalytic activities of sulfur atoms in amorphous molybdenum sulfide for the electrochemical hydrogen evolution reaction, ACS Catal. 6 (2016) 861–867, http://dx.doi.org/10.1021/acscatal.5b02369.

[15] A. Ambrosi, M. Pumera, Templated electrochemical fabrication of hollow molybdenum sulfide microstructures and nanostructures with catalytic properties for hydrogen production, ACS Catal. 6 (2016) 3985–3993, http://dx.doi.org/10.1021/acscatal.6b00910.

[16] H. Zhu, M. Du, M. Zhang, M. Zou, T. Yang, S. Wang, et al., S-rich single-layered

MoS$_2$ nanoplates embedded in N-doped carbon nanofibers: efficient co-electro-catalysts for the hydrogen evolution reaction, Chem. Commun. 50 (2014) 15435–15438, http://dx.doi.org/10.1039/c4cc06480a.

[17] Y. Guo, X. Zhang, X. Zhang, T. You, Defect- and S-rich ultrathin MoS$_2$ nanosheet embedded N-doped carbon nanofibers for efficient hydrogen evolution, J. Mater. Chem. A 3 (2015) 15927–15934, http://dx.doi.org/10.1039/C5TA03766B.

[18] N. Mohamad Latiff, L. Wang, C.C. Mayorga-Martinez, Z. Sofer, A.C. Fisher, M. Pumera, Valence and oxide impurities in MoS$_2$ and WS$_2$ dramatically change their electrocatalytic activity towards proton reduction, Nano 8 (2016) 16752–16760, http://dx.doi.org/10.1039/C6NR03086F.

[19] R.J. Toh, Z. Sofer, J. Luxa, M. Pumera, Ultrapure molybdenum disulfide shows enhanced catalysis for hydrogen evolution over impurities-doped counterpart, ChemCatChem 9 (2017) 1168–1171, http://dx.doi.org/10.1002/cctc.201601561.

[20] H.A. Burch, M. Isaacs, K. Wilson, R.E. Palmer, N.V. Rees, Electrocatalytic re-generation of atmospherically aged MoS$_2$ nanostructures via solution-phase sulfi-dation, RSC Adv. 6 (2016) 26689–26695, http://dx.doi.org/10.1039/C6RA03326A.

[21] D. Escalera-López, R. Griffin, R.E. Palmer, N.V. Rees, MoS$_2$ and WS$_2$ nanocone ar-rays: influence of morphology on the hydrogen evolution electrocatalytic activity and mass transport, Nanoscale (2017) (in review).

[22] K. Seeger, R.E. Palmer, Fabrication of ordered arrays of silicon nanopillars in silicon pillars, J. Phys. D. Appl. Phys. 32 (1999) L129–L132, http://dx.doi.org/10.1088/0022-3727/32/24/102.

[23] K. Seeger, R.E. Palmer, Fabrication of silicon cones and pillars using rough metal films as plasma etching masks, Appl. Phys. Lett. 74 (1999) 1627–1629, http://dx.doi.org/10.1063/1.123638.

[24] A. Wellner, P.R. Preece, J.C. Fowler, R.E. Palmer, Fabrication of ordered arrays of silicon nanopillars in silicon-on-insulator wafers, Microelectron. Eng. 5758 (2001) 919–924, http://dx.doi.org/10.1088/0022-3727/32/24/102.

[25] H.A. Burch, A. Abdela, N.V. Rees, R.E. Palmer, Nanostructured MoS$_2$ arrays for the hydrogen evolution reaction by nanosphere lithography and plasma etching, Nanotechnology (2017) (in review).

[26] M.C. Henstridge, R.G. Compton, Mass transport to micro- and nanoelectrodes and their arrays: a review, Chem. Rec. 12 (2012) 63–71, http://dx.doi.org/10.1002/tcr.201100032.

[27] R.S. Nicholson, Theory and application of cyclic voltammetry for measurement of electrode reaction kinetics, Anal. Chem. 37 (1965) 1351–1355, http://dx.doi.org/10.1021/ac60230a016.

[28] R.J. Klinger, J.K. Kochi, Electron-transfer kinetics from cyclic voltammetry. Quantitative description of electrochemical reversibility, J. Phys. Chem. 85 (1981)

1731–1741, http://dx.doi.org/10.1021/j150612a028.

[29] S.J. Konopka, B. McDuffie, Diffusion coefficients of ferri- and ferrocyanide ions in aqueous media, using twin-electrode thin-layer electrochemistry, Anal. Chem. 42 (1970) 1741–1746, http://dx.doi.org/10.1021/ac50160a042.

[30] T.J. Davies, R.G. Compton, The cyclic and linear sweep voltammetry of regular and random arrays of microdisc electrodes: theory, J. Electroanal. Chem. 585 (2005) 63–82, http://dx.doi.org/10.1016/j.jelechem.2005.07.022.

[31] A. Katrib, F. Hemming, P. Wehrer, L. Hilaire, G. Maire, The multi-surface structure and catalytic properties of partially reduced WO$_3$, WO$_2$ and WC + O$_2$ or W + O$_2$ as characterized by XPS, J. Electron. Spectrosc. Relat. Phenom. 76 (1995) 195–200, http://dx.doi.org/10.1016/0368-2048(95)02451-4.

[32] A.P. Shpak, A.M. Korduban, L.M. Kulikov, T.V. Kryshchuk, N.B. Konig, V.O. Kandyba, XPS studies of the surface of nanocrystalline tungsten disulfide, J. Electron. Spectrosc. Relat. Phenom. 181 (2010) 234–238, http://dx.doi.org/10.1016/j.elspec.2010.05.030.

[33] T. Yukawa, K. Kuwabara, K. Koumoto, Electrodeposition of CuInS$_2$ from aqueous solution (II) electrodeposition of CuInS$_2$ film, Thin Solid Films 286 (1996) 151–153, http://dx.doi.org/10.1016/S0040-6090(96)08545-8.

[34] A.Y.S. Eng, A. Ambrosi, Z. Sofer, P. Simek, M. Pumera, Electrochemistry of tran-sition metal dichalcogenides: strong dependence on the metal-to-chalcogen com-position and exfoliation method, ACS Nano 8 (2014) 12185–12198.

[35] X. Chia, A. Ambrosi, Z. Sofer, J. Luxa, M. Pumera, Catalytic and charge transfer properties of transition metal dichalcogenides arising from electrochemical pre-treatment, ACS Nano 9 (2015) 5164–5179.

[36] E.J.F. Dickinson, J.G. Limon-Petersen, N.V. Rees, R.G. Compton, How much sup-porting electrolyte Is required to make a cyclic voltammetry experiment quantita-tively "diffusional"? A theoretical and experimental investigation, J. Phys. Chem. C 113 (2009) 11157–11171.

[37] D. Escalera-López, Y. Niu, J. Yin, K. Cooke, N.V. Rees, R.E. Palmer, Enhancement of the hydrogen evolution reaction from Ni-MoS$_2$ hybrid nanoclusters, ACS Catal. (2016) 6008–6017, http://dx.doi.org/10.1021/acscatal.6b01274.

[38] B. Seo, H.Y. Jeong, S.Y. Hong, A. Zak, S.H. Joo, Impact of a conductive oxide core in tungsten sulfide-based nanostructures on the hydrogen evolution reaction, Chem. Commun. 51 (2015) 8334–8337, http://dx.doi.org/10.1039/C5CC02472B.

[39] M. Zafir, Mohamad Nasir, Z. Sofer, M. Pumera, Effect of electrolyte pH on the in-herent electrochemistry of layered transition-metal dichalcogenides (MoS$_2$, MoSe$_2$, WS$_2$, WSe$_2$), ChemElectroChem 2 (2015) 1713–1718, http://dx.doi.org/10.1002/celc.201500259.

[40] K. Osseo-Asare, Solution chemistry of tungsten leaching systems, Metall. Trans. B 13 (1992) 555–564, http://dx.doi.org/10.1007/BF02669168.